Available online at www.sciencedirect.com
SCIENCE DIRECT®
Journal of Hydrology 273 (2003) 139–154
Journal of Hydrology
www.elsevier.com/locate/jhydrol

Simulating surface and subsurface initiation of macropore flow

Markus Weiler[a,*], Felix Naef[b,1]

[a]Department of Forest Engineering, Orgeon State University, Corvallis, OR 97331-5706, USA
[b]Institute of Hydromechanics and Water Resources Management, HIF C 44, Swiss Federal Institute of Technology Zürich, CH-8093 Zürich, Switzerland

Received 25 January 2002; revised 7 November 2002; accepted 8 November 2002

Abstract

Initiation of macropore flow either from the soil surface or from a saturated soil layer at depth is a first order control on water flow in macropores and water transfer from macropores into the surrounding soil matrix. Nevertheless, these initiation processes have not been well documented. We surveyed surface topography at four field sites with permanent grass vegetation with grid spacing of 10 cm and applied Kriging to derive the spatial correlation structure. We then simulated the water flux into macropores based on different combinations of surveyed surface micro-topographies, spatial earthworm burrow distributions, and the soil properties, to examine more fully the role of macropore drainage area (MDA) on macropore flow initiation. The spatial distributions of the earthworm burrows were derived from horizontal soil sections extracted from each study profile. The MDA was calculated for different sets of surface topography and macropore density using a flow accumulation algorithm. The resulting MDA of each macropore was used to calculate the total relative MDA, which is equal to the proportion of overland flow draining into macropores, and the MDA probability distribution. The results showed that the macropore density primarily controlled the total MDA and that surface micro-topography strongly influenced the probability distribution of the MDA. Only a few macropores contributed significantly to the total macropore flow whereas the majority of macropores received little water; a phenomenon especially pronounced for a rough surface topography and for a low soil surface gradient. The simulated probability distribution of subsurface initiation was very different from the distribution derived for surface initiation; more symmetrical, less variable and slightly influenced by the roughness and the gradient of the interface between the saturated and the low permeable soil layer. We conclude that the different amount of water supplied to each macropore further alters the percolation depth and transport of solutes in macroporous soils and should be considered for modelling infiltration in macroporous soils.

Keywords: Macropore flow; Micro-topography; Preferential flow; Earthworm burrows; Infiltration

1. Introduction

Macropores influence the infiltration of rainfall and therefore runoff and solute transport in natural soils, in which these structures are common (Larson, 1999). Infiltrating water flows rapidly in structural pore spaces such as worm channels, shrinking cracks, and

* Corresponding author. Tel.: +1-541-737-8719; fax: +1-541-737-4316.
E-mail addresses: markus@2hydros.de (M. Weiler), naef@ihw.baug.ethz.ch (F. Naef).
[1] Tel.: +41-1-633-3384; fax: +41-1-633-1224.

0022-1694/03/$ - see front matter © 2003 Elsevier Science B.V. All rights reserved.
PII: S0022-1694(02)00361-X

root holes and can subsequently bypass portions of the soil profile. The impact of macropores is governed primarily by the water supply to macropores, the water flow in macropores, and the water transfer from the macropores into the surrounding soil matrix (Beven and Germann, 1982; Faeh et al., 1997; Buttle and House, 1997). The causes and extent of preferential flow and particularly macropore flow, which is a subset of preferential flow, are poorly known (Flühler et al., 1996). In particular, the controls on vertical macropore flow by surface and subsurface initiation should be further examined.

This study concentrates on macropore systems caused by earthworm activity, a prime macropore generating factor in natural soils in many climatic regions. Especially the anecic earthworm species *Lumbricus terrestris* generates vertically oriented, highly continuous channels (e.g. Langmaack et al., 1999). Different experimental studies have shown that the maximum flow rate in macropores that are built by anecic earthworm species lies within a narrow range of $1-7\ cm^3\ s^{-1}$ (Bouma et al., 1982; Wang et al., 1994; Shipitalo and Gibbs, 2000). The surveyed macropore density varies between 45 and $700\ m^{-2}$ depending on vegetation, climate, soil management, etc. (Ehlers, 1975; Trojan and Linden, 1998; Munyankusi et al., 1994; Zehe and Flühler, 2001). If we assume a low macropore density of $100\ m^{-2}$, the total possible flow rate of the macropore system ranges from 360 to $2520\ mm\ h^{-1}$. These rates are many times that of naturally occurring rainfall intensities. Thus, the flow rate of the macropore system itself is usually not a limiting factor during the infiltration process, and may in fact be a process enhancing infiltration (Weiler, 2001).

Macropore flow initiation during infiltration is a function of initial matrix water content, rainfall intensity, rainfall amount, matrix hydraulic conductivity, and soil surface contributing area (Trojan and Linden, 1992). Water can flow into macropores either from the soil surface or from a saturated or partially saturated soil layer at depth. Subsurface initiation of macropore flow occurs only if specific arrangements and properties of the soil exist that allow for interaction between matrix water and the macropore void space (Ela et al., 1992; Li and Ghodrati, 1997; Weiler et al., 1998). Whilst some studies have shown that macropore density, slope, and roughness of the surface influence the surface initiation (Trojan and Linden, 1992; Léonard et al., 1999), the controls on macropore flow initiation, infiltration and solute transport are still not well understood.

Few studies have directly observed or quantified macropore initiation. Laboratory experiments cannot reproduce the complex natural relations between the soil surface, the vegetation, and the macropores. Artificial macropores are often only useful to study a selected detail of the initiation process (e.g. Phillips et al., 1989). However, some laboratory experiments with grid lysimeters, which measure the outflow variability below a soil block in a grid collector system, have shown that flow in macropores can be highly variable, probably due to a variable initiation of macropore flow (Andreini and Steenhuis, 1990; Shipitalo et al., 1990; Edwards et al., 1992; Bowman et al., 1994; Quisenberry et al., 1994). Field measurements to directly observe surface initiation are difficult or even impossible because vegetation often covers the surface and thus prevents visual observation and recording. Removing the vegetation cover alters the surface characteristics and the infiltration controls that one seeks to measure. Indirect measurements of the soil water content and the matric potential in combination with dye experiments may only verify whether macropore initiation has taken place at the soil surface or within the soil (Weiler and Naef, 2002).

This paper describes a new approach to measure and simulate the initiation of water flux into macropores from both the soil surface and subsurface layers. We surveyed the surface topography and the earthworm generated macropore distributions on four field sites and used these data to calculate the surface area draining into each macropore. The resulting flow rate distributions in the macropores are then assessed and the main controls of the initiation process are systematically analysed for surface and subsurface initiation. Specifically our objectives were:

1. How does the macropore density influence the total MDA and thus the infiltration behaviour of soils for surface initiation?
2. How do the macropore density, the hillslope gradient, and the surface roughness influence the MDA probability distribution and thus the flow rate distribution in the macropores for surface initiation?

3. How do macropore density, spatial variable saturated hydraulic conductivity, and spatial variable soil horizon boundaries influence the initiation probability distribution under non-steady state conditions for subsurface initiation and how does the non-steady state simulations compare to the steady state solution?
4. How compares the resulting macropore flow rate distribution of surface initiation to subsurface initiation?

Finally, simulation results are compared with findings from sprinkling and dye tracer experiments (Weiler and Naef, 2002) and various other published laboratory experiments. Implications on water and solute transport in soils with macropores are discussed.

2. Methods

2.1. Field sites

The soil surface topography and the macropore distribution data were collected from four field sites in Switzerland. On these sites the processes and regulation mechanisms of macropore flow with respect to infiltration have been extensively studied with combined sprinkling and dye tracer experiments with different rainfall intensities and initial soil moisture conditions (Weiler, 2001; Weiler and Naef, 2002). All sites have been covered by grassland for at least 20 years. Thus, they provide an undisturbed record of the macropore network development by earthworm activity in the soil (Syers and Springett, 1983). Table 1 summarizes the sites' soil properties, soil classification, geological parent material, and soil properties of individual soil horizons.

2.2. Surface topography characterization

A detailed examination of the micro-topography of the soil surface is a prerequisite for simulating macropore flow initiation at the soil surface. We manually surveyed the soil surface topography for an area of 290 cm by 100 cm at each of the four sites using a grid spacing of 10 cm. Table 2 summarizes the average slope and the 'deviation of the surface from a fitted plane' at each site. Kriging was then applied to increase the spatial resolution of the measured soil surface data. Kriging conserves the spatial correlation of the topography and can incorporate possible anisotropy and underlying trends not apparent in the raw gridded data (Huang, 1998). Because the surface topography was accurately measured, an exact interpolation method like Kriging without nugget effect was used. An experimental variogram was calculated for the four sites, after a plane was fitted to the measured values and subtracted from the values to incorporate the drift of the data (Stein, 1999). Anisotropy was not detected. All experimental variograms showed an exponential behaviour and no nugget effect. Therefore, an exponential model with an anisotropy ratio of one was fitted to the experimental semi-variogram:

$$\gamma(h) = C\left[1 - \exp\left(-\frac{h}{a}\right)\right] \quad (1)$$

where $\gamma(h)$ is the semi-variogram, C is the scale or sill for the structured component of the variogram, a is the range, and h is the separation distance. The derived parameters of the exponential model for the sites are listed in the last two columns of Table 2.

2.3. Spatial macropore distribution

If the stochastic process generating the spatial pattern of macropores is known, initiation can be simulated for different realisations of macropore distributions. The spatial distribution of the macropores at the soil surface and the macropore density were surveyed at each site across four horizontal soil sections 1–2 cm below the surface (details on the preparation of the sections in Weiler, 2001). Photos of the 100 cm by 50 cm sections were taken and macropores larger than 1 mm^2 were classified using image analysis (Weiler, 2001). The spatial pattern of macropores and the related distribution of distances from a point to the nearest macropore are important properties influencing initiation and macropore-enhanced infiltration (Droogers et al., 1998). The nature of the processes generating a point pattern can be evaluated with quadrate analysis (Smettem and Collis-George, 1985; Brimicombe and Tsui, 2000). The Index of Cluster Size (ICS), which can be

Table 1
Soil properties of the experimental sites

Site	Soil classification [a]	Geological parent material	Average values for distinct soil horizons				
			Depth (cm)	Density (g cm^{-3})	Soil texture [b]	K_{sat} [c] (mm h^{-1})	n_{mac} [d] (mm^{-2})
Rietholz-bach	Mollic Cambisol	Conglo-merates (molasse)	0–30	1.14	Loam	12.0	95
			30–60	1.25	Loam	9.6	155
			60–100	1.35	Clay loam	4.7	90
Heiters-berg	Umbric Cambisol	Moraine	0–20	1.34	Loam	6.5	210
			20–45	1.57	Loam	1.9	140
			45–100	1.66	Loam	1.4	93
Koblenz	Eutric Cambisol	Moraine	0–15	1.31	Silt loam	10.7	154
			15–45	1.35	Silt loam	3.8	196
			45–90	1.51	Loam	2.1	88
Nieder-weningen	Eutric Cambisol	Sandstone (molasse)	0–30	1.41	Sandy clay loam	15.4	186
			30–55	1.44	Sandy loam	29.3	322
			55–100	1.42	Sandy loam	54.8	185

[a] Food and Agricultural Organization (1974)
[b] Soil Survey Staff (1951)
[c] Saturated hydraulic conductivity of the soil matrix determined from soil texture and bulk density (Schaap and Leij, 2000)
[d] Macropore density was determined from macropore with an area larger than 1 mm^2 and a circular shape using image analysis of the horizontal soil sections (Weiler, 2001)

calculated from the point counts in each quadrate, is a straightforward method to account for this generation process:

$$\mathrm{ICS} = \frac{s^2}{\bar{x}} - 1 \qquad (2)$$

where $\bar{x}$ is the mean and s^2 is the variance of the counts in each quadrate. An ICS > 0 shows the existence of clustered pattern, ICS < 0 implies a uniform pattern, and ICS $= 0$ indicates a random pattern. The ICS depends on the quadrate size (if the data set is not synthetic) because the generation process of non-synthetic data is usually scale dependent.

In this study, macropores classified from the horizontal sections were used to calculate the ICS. Verification of the image analysis procedure resulted in correct classification of 90% of the macropores (Weiler, 2001). To account for scale effects, the size of the quadrates were varied calculating the ICS. The centre of each classified macropore was determined and the resulting point pattern was used to derive the ICS. Table 3 shows the average ICS for each site of the four horizontal sections. The values show that the underlying generation process of the macropore pattern is random except for large quadrates where the point pattern tends to be more clustered. The higher values for large quadrate sizes at the Koblenz

Table 2
Characterisation of the surface topography of the four experimental sites

Site	Slope (%)	Absolute deviation of the surface (mm)				Variogram	
		Average	Median	25% quantile	75% quantile	a (cm)	C
Rietholzbach	22.1	7.8	6.0	3.0	10.9	43.8	1.35
Heitersberg	22.9	6.6	5.5	2.5	9.1	93.1	1.90
Koblenz	16.4	14.6	10.1	4.4	18.1	42.5	1.34
Niederweningen	16.2	14.0	8.0	3.6	14.4	26.8	1.16

Table 3
Average Index of Cluster Size (ICS) for each site with a variable quadrate size

Site	Index of Cluster Size (ICS) for quadrate size			
	5 cm	10 cm	30 cm	50 cm
Rietholzbach	0.003	0.025	0.053	0.073
Heitersberg	−0.004	0.005	0.084	0.144
Koblenz	−0.006	0.020	0.262	0.558
Niederweningen	0.000	0.037	0.385	0.719

and Niederweningen sites (Table 3) are influenced by ant activity and mouse holes. Notwithstanding, the pattern of the macropores formed by earthworm activity is a random point pattern. Smettem and Collis-George (1985) also showed that spatial patterns of earthworm channels are random for grassland soils. The Poisson process is the simplest possible stochastic mechanism to generate the random spatial distribution of this type of macropore (Diggle, 1983).

2.4. Modelling of surface initiation

With knowledge of the site surface topography, the macropore density, and the spatial pattern of the macropores near the soil surface, a description and simulation of the soil surface macropore initiation was sought. If one assumes steady state conditions, uniform rainfall distribution, a homogeneous hydraulic conductivity of the soil matrix around the macropores, and that the surface topography is not affected by the rain itself, then the rainfall not infiltrating into the soil matrix flows according to the soil topography. If the water flows into a macropore open at the surface, it will completely 'disappear' since the vertical flow rate in a single earthworm channel is large relative to the surface flow (Weiler, 2001). Consequently, the area that drains to a macropore (i.e. the local upslope contributing area of the vertical hole opening) determines the amount of water flowing in the macropore. Thus, the inflow quantity of each macropore is proportional to its macropore drainage area (MDA). The inflow q (mm h^{-1}) into a macropore i is then given as:

$$q_i = (p - i_{mat})\mathrm{MDA}_i\, n_{mac} \quad (3)$$

with the rainfall intensity p (mm h^{-1}), the infiltration rate into the soil matrix i_{mat} (mm h^{1}), and the macropore density n_{mac} (mm^{-2}).

We assessed the MDA for a given soil surface and macropore density with the following steps: (1) The surface topography (with a grid spacing of 1 cm) was either interpolated from the surveyed topography using Kriging with derived parameter for the exponential model (Table 2) or was generated randomly with a sequential Gaussian simulation program in GSLIB (Deutsch and Journel, 1992). The chosen grid spacing of 1 cm corresponds to the average opening size of an earthworm burrow at the soil surface. (2) The interpolated or generated topography was then overlaid with a rough surface representing the micro-topography. The micro-topography represented the roughness formed by vegetation, soil aggregates, or the activity of the earthworms, which often form a midden around the burrows by defecating soil particles and organic debris (Syers and Springett, 1983). As details about the micro-topography are generally unknown, a normally distributed random field with a standard deviation of 1 mm was used to reproduce this micro-topography. The flow direction of every cell of the 'new surface' was then calculated. The extent of depressions was determined iteratively starting at a local minimum (no flow cell). A depression was defined as the area where ponding could occur. Contiguous depressions were then merged and the topography underlying the depressions was raised to the height of the outlet of the depression.

(3) After a spatially random distribution of macropores for a defined macropore density was generated, the location of macropores was compared to the location of depressions. If a macropore was located within a depression, it was assumed to capture all water flowing into the depression. The flow accumulation for each cell was calculated according to the method of Holmgren (1984):

$$A_i = \frac{A(\tan \beta_i L_i)^h}{\sum_{i=1}^{n} (\tan \beta_i L_i)^h} \quad (4)$$

where n is the total number of downhill directions, A_i is the amount passed onto the ith downhill cell, A is the total up-slope area accumulated in the current cell,

tan β_i is the gradient and L_i is the contour length in the ith downhill cell and h is a weighting factor. If $h = 1$, the multiple-flow-direction algorithm by Quinn et al. (1991) was used. For $h > 100$, the single-flow-direction algorithm was implemented. We assumed dispersive flow at the soil surface, where h was set to two. After the flow accumulation for a macropore cell was calculated, the actual accumulated area was transferred to the macropore cell. This value was then the MDA of the macropore. The flow accumulation of this surface cell was then set to zero.

In order to reduce the influence of the boundary condition (no flow cell), only the MDA of the macropore cells located in the lower downslope half of the soil surface were considered (Weiler, 2001). The MDA of each macropore was normalized by the mean MDA; that is the surface area was multiplied by the macropore density. The normalized MDA of all macropores was then either summed up to calculate the total relative MDA or the cumulative probability distribution was derived. To account for different spatial distributions of the simulated macropores, 20 realizations with different macropore distributions were derived for each of the four surface topographies.

2.5. Modelling of subsurface initiation

Our general approach for modelling subsurface initiation was similar to the surface initiation model. We considered a soil layer boundary with a sharp contrast in hydraulic conductivity where water excess would be generated and where, in this case, the water would flow under saturated conditions to macropore openings (themselves spatially randomly distributed and defined by the macropore density). In contrast to the surface initiation model, water flow is driven by the water table gradient, since the hydraulic head in the macropore is zero. A perched water table is built within a soil layer by the excess water, that is the difference between the recharge into the soil layer and the percolation from this layer. In addition to the surface initiation model, non-steady state conditions had to be considered as the amount of water stored in the porous media increases with time until the system reaches steady state conditions.

These prerequisites were accommodated by laterally routing flow in a saturated layer above a low permeable layer under Dupuit-Forchheimer assumptions. The explicit grid-by-grid cell approach of Wigmosta and Lettenmaier (1999) was used for this routing. In contrast to most of the existing models defining the flow direction a priori by the surface topography, our approach recalculates the flow direction and outflow from each grid cell for each time step based on the local water table gradient.

The model was parameterized to account for a variety of factors that could change subsurface initiation. The parameters themselves were based on field measurements or observations. The reference simulation A (Table 4) was run with a macropore density (n_{mac}) of 250 m^{-2}, which is in the upper half of the observed range of macropore density (Table 1), but representing an average value of other studies. The spatially uniform saturated hydraulic conductivity (k_s) is based on an average value estimated for the upper soil layers of the field sites (Table 1). The slope of the lower boundary was set to zero without topographic variations, conceptualized as a sharp, plane interface between two soil layers. For all simulations, the overall dimensions of the domain was set to 1 m by 1 m with a grid spacing of 1 cm. Each spatially random generated macropore was represented in the model by one grid cell with a hydraulic head of zero. The drainable porosity (effective porosity or specific yield) was set to 10%. Build up of the saturated zone in the modeled soil layer was driven by a recharge event of 3 h duration with a recharge intensity of 2 mm h^{-1}, thus representing constant infiltration under unsaturated conditions (2–5 mm h^{-1}). This layer of interest lies over a low permeable soil layer with an actual percolation rate between 0 and 3 mm h^{-1}. Three of four of the field sites in Switzerland exhibited such conditions. After the recharge event, the recession was simulated for another 5 h. Four additional simulations (B–E in Table 4) were run, where one of the following parameters was changed to explore possible influence factors: macropore density, spatial variability of saturated hydraulic conductivity, slope of the lower boundary, and roughness of the lower boundary. Hydraulic conductivity was varied applying a lognormally distributed spatially random conductivity field. The roughness of the lower boundary and thus the interface between the high and low permeable soil layer was described similarly to the generated surface

Table 4
Parameter settings for subsurface initiation model

Simulation	n_{mac} (m^{-2})	k_s (mm h^{-1})	Slope (%)	Lower boundary
A	250	6.0	0	Plane
B	100	6.0	0	Plane
C	250	6.0(±1.3)	0	Plane
D	250	6.0	30	Plane
E	250	6.0	0	Rough ($\sigma = 10$ mm, $a = 20$ cm)

within the surface initiation model using an exponential variogram model.

In addition, we also tested the conditions under which a steady state assumption, and thus a simpler model, could be used to predict the MDA and thus the distribution of macropore flow initiation. For uniform hydraulic conductivity, steady state conditions, and a horizontal and plane boundary between the two soil layers, a macropore will drain the area that is closest to it in order to maximize gradient. This partition of the MDA can be described by the Voronoi diagram (Thiessen polygons) (see details in Aurenhammer, 1991). If a Poisson process is used to describe the spatially random distribution of macropores and the areal density of the generated random points, λ is equal to the macropore density, the size distribution of the MDA is equal the size distribution of random Voronoi segments that can be derived for one dimension (Kiang, 1966):

$$f(x) = \frac{c}{\Gamma(c)}(cx)^{c-1}e^{-cx} \quad (5)$$

where the Gamma distribution has the shape parameter $c = 2$ for the 1-D case and x is the normalized length. For the two dimensional case, the distribution becomes difficult to establish and no rigorously derived result has been published in the literature to date. However, simulations with randomly generated point patterns showed that for every areal density λ, c is equal to 4. (Kiang, 1966).

3. Results

The simulation results for surface initiation are presented for the measured surface topography and for the simulated surface topography. The effect of the macropore density on total MDA and on the MDA probability distribution is assessed for the measured topography of the four sites. For the simulated surface topography the effects of the hillslope gradient on the MDA probability distribution are presented. The simulation results for subsurface initiation are described for the five different parameter sets in order to evaluate factors influencing the probability distribution of macropore initiation. Furthermore, the results of the dynamic simulations are compared with the steady state assumption that water in a saturated soil layer will flow to the nearest macropore. Finally, the distributions for surface and subsurface initiation are compared.

3.1. Surface initiation: macropore density and total MDA

The flow accumulation patterns at the soil surface with the MDA for each macropore for four selected realizations are shown in Fig. 1 and will be used in the following to explain some findings. If the macropore density is low, the probability for water flowing on the soil surface to drain into a macropore is also low. Therefore, how strongly does the macropore density influence the MDA and thus the infiltration behaviour of the soil? For the four sites, the influence of the macropore density on the relative total MDA is illustrated in Fig. 2. The error bars result from the 20 realizations for different spatial distributions of the simulated macropores. For comparison, the values of a plane surface with a gradient of 20% are shown. Especially for a density below 200 m^{-2}, the macropore density strongly influences the total relative MDA. Generally, the relationship was quite similar for the four sites. For macropore density between 100 and 250 m^{-2}, the Koblenz and Niederweningen sites in particular showed higher values. These two sites featured a higher absolute deviation of the surface from a fitted plane. This deviation was expressed as a higher surface roughness than the other two sites (Table 2). Fig. 1 shows the flow accumulation pattern at the soil surface for the Rietholzbach and Koblenz site and illustrates, quantitatively, a possible explanation for the differences. For low roughness surface topography (Rietholzbach), a higher number of individual flow channels in hollows are observable

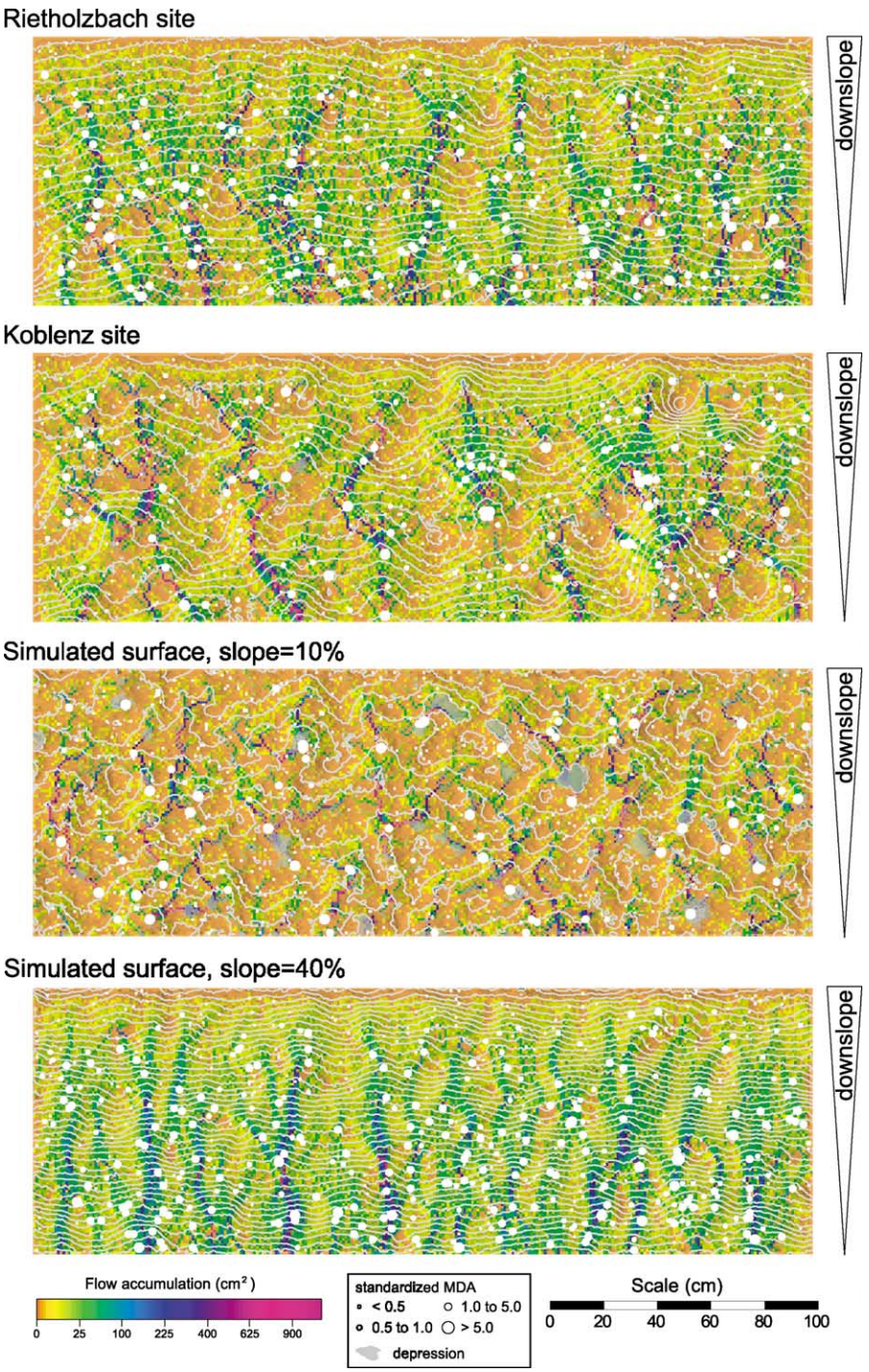

Fig. 1. Flow accumulation pattern at the soil surface for two surveyed sites (Rietholzbach and Koblenz) and for two simulated surfaces. Grey lines are the contours with an elevation distance of 1 cm. The size of the macropore drainage area (MDA) for individual macropores is superimposed by white dots.

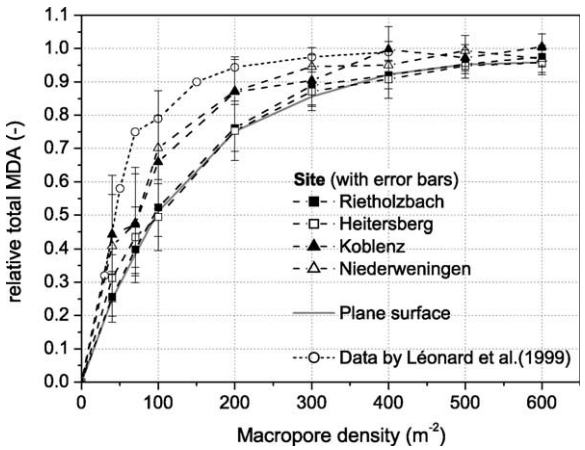

Fig. 2. Influence of macropore density on relative total macropore drainage area.

than for the high roughness surface topography (Koblenz). If the macropore density is low, the probability that macropores drain all flow channels is thus lower for the site with many flow channels. Therefore the total relative MDA is higher for the high roughness surface topography sites. The results for the low roughness surface topography are comparable to the MDA of a plane surface. Léonard et al. (2001) also derived a relation for macropore density and total MDA with a hydraulic model solving the 2-D St.Venant equation. Their values, which are similar to our results, are also shown in Fig. 2 and support the use of our approach to simulate the initiation process.

3.2. Surface initiation: macropore density and MDA probability distribution

Given our findings with macropore density and total MDA, we expected that the MDA probability distributions could show different behaviours. Fig. 3 shows the cumulative probability distribution of the MDA for different macropore densities at the four sites. Again, a difference between the low roughness surface topography sites (Rietholzbach and Heitersberg) and the high roughness surface topography sites (Koblenz and Niederweningen) are evident. For low roughness topography, the MDA was less than ~0.5 times the expected MDA for 50% of the macropores and the MDA was less than the expected MDA for 70% of the macropores. For high roughness topography, however, the MDA was less than ~0.5 times the expected MDA for 70% of the macropores and the MDA was less than the expected MDA for 85% of the macropores. Furthermore, the MDA was more than 5 times larger than the expected MDA for only 2% of the macropores for the low roughness topography compared to over 4% for the high roughness topography. These differences can again be seen in Fig. 1. For low roughness topography, the channelling is low and thus only a few macropores receive a higher MDA. For high roughness topography, the channelling is high and thus macropores in the channels receive a high MDA. For all sites, the influence of the macropore density on the probability distribution is minor. There was a general trend that the cumulative probability distribution shifted to higher values if the normalized MDA was below two, but shifted to lower values if the normalized MDA was above two. This change could be related to the occurrence of high flow accumulation values. If the macropore density is low, the probability for high flow accumulation values is high. Thus, if a macropore is located within a hollow, its MDA is also high. However, as the channelling is more pronounced for a low macropore density, the macropores will have a lower MDA if their location is not in a hollow.

3.3. Surface initiation: hillslope gradient and MDA probability distribution

We used the results of the simulated surface topography to study the effects of the hillslope gradient. The simulated surface had similar spatial characteristics as the Rietholzbach and Koblenz sites with an underlying exponential model of scale $C = 1.35$ and range $a = 42$ cm. This simulated surface was then altered by changing the average deviation of the surface from a plane to 7 and 14 mm (similar to the observed values for the low and high roughness surface topography) and by introducing gradients from 0 to 40%. The results for the cumulative probability distributions are shown in Fig. 4. The distributions represent the average for the same four different macropore densities shown in Fig. 3. For the low roughness topography (Fig. 4(a)), the slope determined strongly the probability distribution. If the surface was flat or only slightly inclined (0–10%), 60% of the macropores drained an area smaller than 0.1 times the expected MDA, however,

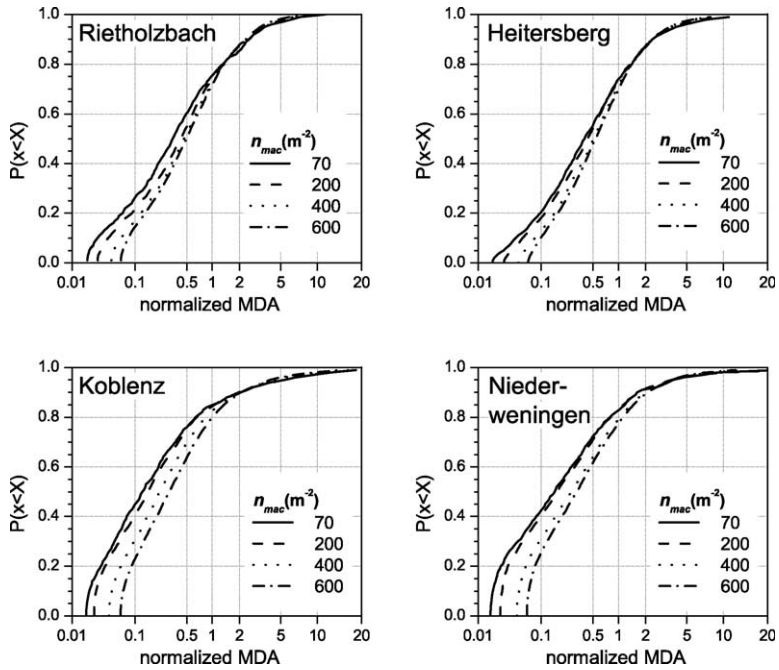

Fig. 3. Cumulative probability distributions for surface initiation of macropore drainage area for different macropore densities at the four sites (a) Rietholzbach, (b) Heitersberg, (c) Koblenz, and (d) Niederweningen.

around 2% of the macropores drained an area larger than 10 times the expected value. If the gradient was steep (40%), over 40% of the macropores drained an area between 0.5 and 2 times the expected value with only a few macropores that drained an area that was smaller than 0.1 times and larger than 5 times the expected MDA. The reason for this difference is visually apparent in Fig. 1. If the gradient is low (Fig. 1(c)), water flows into the nearest hollow, where the water accumulates. A macropore located in the depressions receives a very high MDA, however, a macropore located on the ridge receives only a very low MDA. Because the total area with a low flow accumulation (<5 cm^2) is high, the probability is high that macropores are within this area. In contrast, the flow accumulation pattern looks different for the surface with a steep gradient (Fig. 1(d)). Because the roughness is low compared to the overall slope, water flows mainly in the direction of the slope and is channelled into the 'valleys'. The area with

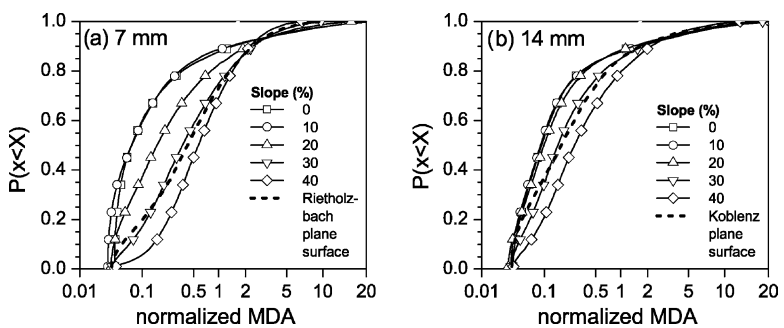

Fig. 4. Influence of the slope on the cumulative probability distribution for surface initiation of the macropore drainage area with (a) 7 mm average deviation and (b) 14 mm average deviation of the surface.

intermediate flow accumulation (5–30 cm^2) is high as water from higher elevation flows over a longer distance to lower elevation. Thus, the probability is high that macropores drain this intermediate flow accumulation. The probability for high MDA decreases as the channelling of water in the downslope direction is more frequent. Comparing the results for the two different surface roughness conditions (Fig. 4(a) and (b)), the influence of the gradient is lower for the high surface topography. However, the same general pattern as in Fig. 4(a) is also valid for Fig. 4(b). The influence of the slope probably decreases because the water flows more directly into a depression or hollow, if the roughness of the soil surface is higher.

Fig. 4 also illustrates the distributions from the Rietholzbach and Koblenz sites for the measured topography with the results from the simulated surface topography. The average cumulative probability distribution for the Rietholzbach site matches the distribution for the simulated low roughness surface in Fig. 4(a) for a gradient of 30%. This value is higher than the measured gradient of 22% for the Rietholzbach site (Table 2), however, the general behaviour is similar for the measured and simulated surface topographies. The same results were found comparing the results of the site Koblenz with the simulated high roughness surface in Fig. 4(b). The distribution also matches best with the simulation results for a slope of 30%, despite a lower measured slope of only 16% for the site. In addition, the cumulative probability distribution calculated for a plane slope (Fig. 4) does not additionally influence the distribution. The resulting distribution is similar to a normal distribution with the median equal to the mean and a symmetrical shape. Consequently, the microtopography at the soil surface considerably changes the distribution of the MDA and thus the initiation of macropore flow.

3.4. Subsurface initiation: dynamic simulation and probability distribution of macropore initiation

Fig. 5 shows the flow from the saturated soil layer into the macropores for the five different simulations. The total flux is nearly similar for all simulations with a macropore density of 250 m^{-2}, and thus independent from the changing state parameters

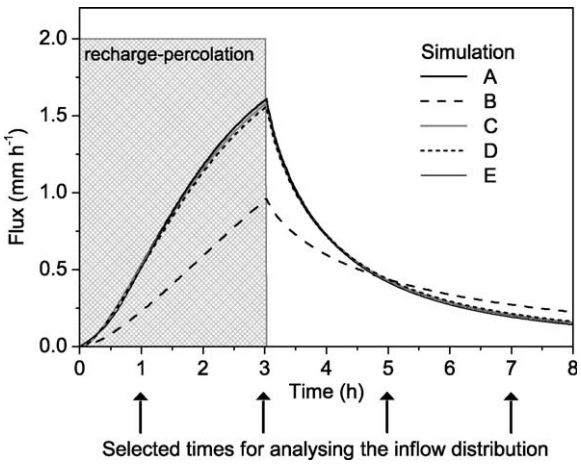

Fig. 5. Total flow from the saturated soil layer into the macropores during 5 different simulations and the selected times at which the probability distribution for subsurface initiation was analysed.

(Table 4). The flux for the simulation with the lower macropore density is lower due to lower average gradients. Fig. 5 also indicates the four selected times for calculating the initiation probability distribution: 1, 3, 5 and 7 h. The resulting normalized cumulative probability distribution for the reference simulation A and the simulation B is shown in Fig. 6. At 1 h, the distribution shows a low variance around the mean and a negative skewness, as the water table gradient towards the macropores is only fully developed in areas with a high macropore density. At 3 h (peak flux) the distribution is more symmetrical. At 5 and 7 h (during the recession after the input ended), the distributions are nearly similar with a positive skewness. If we compare these results to the steady-state assumption (Eq. 5), the distributions during recession match very closely the steady-state assumption. However, during the rising limb and peak, the distributions show a lower variance and different shape. Similar results can be observed for a lower macropore density (Fig. 6(b)). Here the distributions tend to develop slower towards the steady-state distribution, as the average spacing between the macropores is higher. The same results can also be observed for a lower hydraulic conductivity of the soil matrix or lower fluxes. Nevertheless, during recession the inflow distribution again matches closely the solution for steady-state conditions.

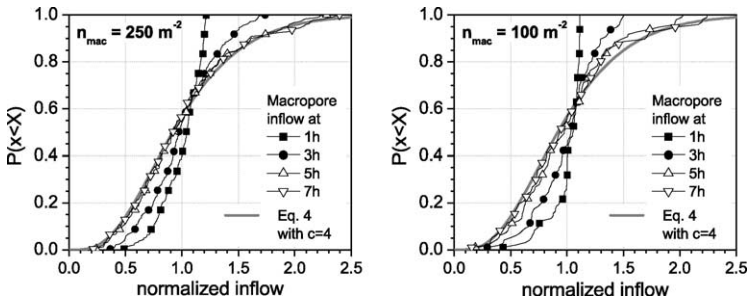

Fig. 6. Cumulative probability distributions of subsurface initiation flow at four selected times for (a) the reference simulation A with a macropore density of 250 m^{-2} and (b) simulation B with a macropore density of 100 m^{-2}.

We then explored other possible influence factors on the probability distribution of macropore initiation. Fig. 7 shows the results for simulation C and E, which used a spatial variable k_s field and spatial variable lower boundary topography, respectively. The variable hydraulic conductivity did not influence the shape of the distributions. Compared to the reference simulation, the shape of the distribution at 1 h was even more similar to the steady state assumption. The results for the simulation with the rough interface between the high and low permeable soil layers show that this factor can influence slightly the shape of the distribution (Fig. 7(b)). For the simulation times of 1 and 3 h, the distributions are quite similar to the steady state assumption. However, during recession, the variance increased resulting in a flatter cumulative probability distribution. For simulation D (slope = 30%), the results are similar to simulation E and therefore not shown in detail. In summary, the derived distributions for subsurface initiation were variable due to the non-steady state behaviour of subsurface initiation. Nevertheless, the solution for the steady state assumption was quite similar to most of the derived distributions for non-steady state.

3.5. MDA distribution for surface and subsurface initiation

Finally, the derived distributions of MDA for surface initiation at the four sites were compared with the distribution for subsurface initiation calculated for non-steady state condition with the explicit grid cell approach and for steady state condition according to Eq. 5 through their frequency distributions (Fig. 8). For surface initiation, the frequency distribution of the MDA showed an exponential behaviour with a high variance. The frequency distribution and therefore the distribution of macropore flow for surface initiation was influenced mainly by the surface topography. Only a few macropores, probably situated in depressions or hollows, contributed significantly to the water flow. The majority of macropores had a very low normalized MDA and thus received small amount of water. Other studies have also showed

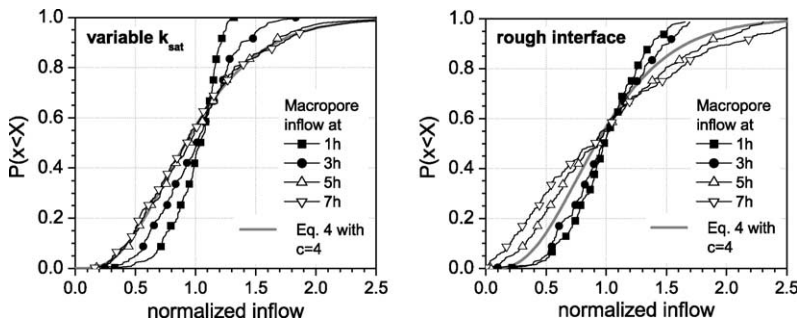

Fig. 7. Cumulative probability distributions of subsurface initiation flow at four selected times for (a) simulation C with a spatially variable saturated hydraulic conductivity field and (b) simulation E with a spatially variable lower boundary topography.

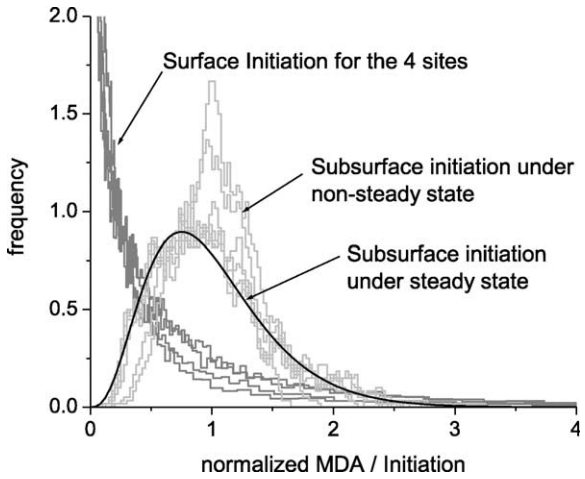

Fig. 8. Frequency distribution of the macropore drainage area for surface and subsurface initiation.

that the distribution of MDA initiated from the surface shows an exponential behaviour (Ela et al., 1992). Trojan and Linden (1992) measured a significant increase of macropore flow in macropores located in micro-depressions, since their MDA was larger than for macropores located on ridges. For subsurface initiation, in our study, the initiation probability distribution was more symmetrical and had a lower variance. The variance was especially small during recharge conditions. For the recession, the dynamic simulation resulted in similar probability distributions as for the steady-state assumption. We conceptualised that the subsurface initiation operates like a filter, equalizing the macropore flow compared to surface initiation, even if the properties of the soil layer are considered spatially variable. In general, macropore initiation provides a different supply of water into each macropore and thus causes a different water flux in each macropore.

4. Discussion

This study assessed the macropore flow initiation process at the surface and within the soil and the resulting flow rate distribution in vertical macropores formed by earthworm activity. We could show that macropore flow initiation results in a different supply of water into each macropore depending on the surface topography, the macropore density, and the gradient of the soil surface. Now, we compare our solely simulation based results to various experimental findings and discuss the potentials to use our results to model water movement and solute transport in macroporous soils.

Combined sprinkling and dye tracer experiments at our four sites by Weiler and Naef (2002) provided one opportunity to observe indirectly the variation of flow rate in the macropores depending on the initiation process. Fig. 9 compares two classified dye patterns from horizontal soil sections. Tensiometer data and dye patterns from vertical sections confirmed that macropore flow was initiated at the soil surface (Fig. 9(a)) and within the topsoil (subsurface initiation) (Fig. 9(b)). The staining around macropores is proportional to the water flow from the macropores into the soil matrix. This interaction, however, depends on the actual flow rate within the macropores. Despite the fact that the total stained area around the macropores is different for the two sites, the variability of the stained area is larger for surface initiation. The dye pattern shows some macropores without staining and a few macropores where the staining is very large. For subsurface initiation, however, the stained areas around the macropores are quite similar. It should be noted that the hydraulic properties of the soil matrix were quite homogeneous for each horizontal soil sections. These differences in the dye patterns are reasonable, if the flow rate in the macropores and thus the interaction is variable depending on the initiation process.

A flow rate distribution within macropores resulting from macropore flow initiation has also been observed in several published laboratory experiments (Andreini and Steenhuis, 1990; Shipitalo et al., 1990; Edwards et al., 1992; Bowman et al., 1994; Quisenberry et al., 1994). In order to study the spatial and temporal variability of water and solute movement through intact soil blocks, it is necessary to interface the block with solution collection systems. Andreini and Steenhuis (1990) and Shipitalo et al. (1990) constructed the first grid lysimeter using a grid collector system. All experiments showed a high variability of water and solute flux among individual grid cells. Andreini and Steenhuis (1990) measured water

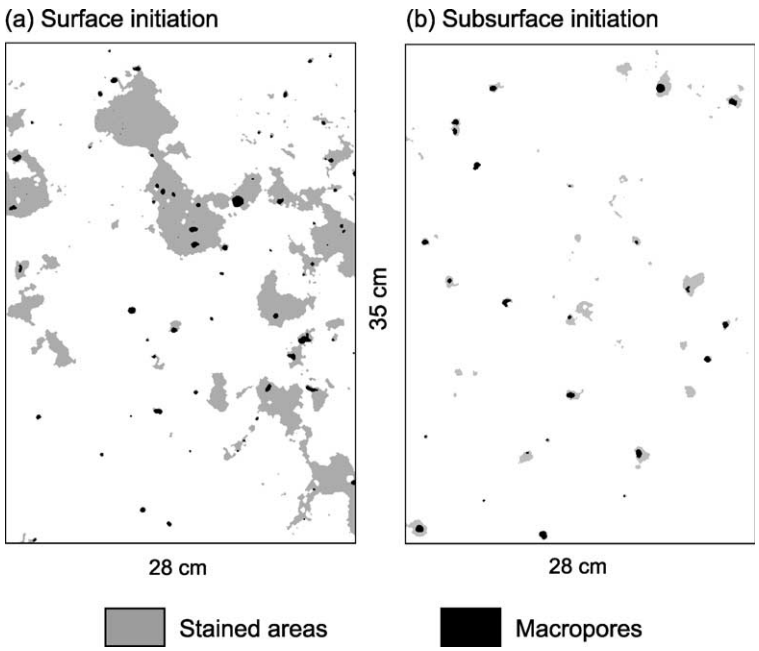

Fig. 9. Classified dye patterns of two horizontal soil sections, where macropore flow is initiated (a) at the soil surface (site Koblenz, $z = 50$ cm) and (b) within the topsoil (subsurface initiation) (site Heitersberg, $z = 40$ cm).

flow from only 30 to 40% of the total grid cells. Bowman et al. (1994) found that over 99% of the water flow was conducted through only about 26% of the basal area of the soil block, regardless of the application rate. They also conducted a bromide tracer experiments and found that approximately 85% of the water in the soil block was bypassed by the bromide. Quisenberry et al. (1994) also used different application rates ($5-31$ mm h^{-1}) and measured water flux and chloride concentration. Macropore flow was initiated at the grass covered soil surface. They found that 50% of the water and chloride appeared within 20% of the cross-sectional area. They always detected one grid cell in which the water flux was 3–30 times higher than the application rate. The water flux measurements of these published experiments correspond to our derived flow rate distribution for surface initiation. Edwards et al. (1992) measured percolate for a soil block with macropores formed by *Lumbricus terrestris* and found one grid cell comprised 30 to 60% of total percolate. Shipitalo and Edwards (1996), who also studied the influence of the initial soil water content, found similar values. They concluded that the number of cells contributing to flow did significantly increase with increasing soil water content and argued that under dry condition macropore flow was initiated at the soil surface, and under wet conditions from a saturated zone near the soil surface.

We have not evaluated the impact of the initiation process for other types of macropores (root channels, cracks) and for other soil surface characteristics (forest, tillage). Furthermore, we have not considered temporally changing soil properties, like soil crust formation, soil erosion, soil management practice, or surface sealing. Also the dynamic of the whole macropore system due to earthworms closing holes and making new ones was not studied in more detail. Nevertheless, we hypothesize that the flow rates in all kind of macropores will not be the same as the area that drains into each macropore is always different. The actual MDA distribution for other types of macropores or soil surface characteristics can be different compared to the presented distributions, but the general approach to quantify their MDA should be

the same. Thus we recommend that the approach outlined in this study be replicated for other types of macropores and other soil surface characteristics to receive a general description of flow rate distribution in macroporous soils. This flow rate distribution should then be considered for modelling infiltration in macroporous soils (Weiler, 2002).

5. Conclusion

We confirm the importance of macropore flow initiation for infiltration and quantified the different amounts of water supplied to each macropore and thus the different water fluxes in each macropore. For surface initiation, the total MDA and therefore the proportion of overland flow that can drain into macropores is strongly influenced by the macropore density. A macropore density of 100 m^{-2}, which is a low value compared to field observations (Weiler and Naef, 2002), is sufficient to capture between 50 and 80% of the overland flow. The probability distribution of the MDA and therefore the distribution of macropore flow from surface initiation is influenced mainly by the surface topography. We found that only a few macropores contribute significantly to the water flow, especially for a irregular and rough surface topography and for a low soil surface gradient. However, these differences are minor compared to the derived distribution for subsurface initiation or compared to the common assumption of the same flow rate in each macropore. The probability distribution of macropore flow for subsurface initiation is more symmetrical and has a lower variance than that for surface initiation. This difference changes slightly depending on the developed gradient of the water table in the saturated soil layer and the heterogeneities in the soil. Independent from these various and related factors, the probability distribution for subsurface initiation is distinctly different from the distribution for surface initiation.

The actual macropore flow distribution probably differs somewhat from the simulated distributions, as macropore flow initiation is a dynamic process and soil properties are often more heterogeneous than the simulations can reproduce. Flow rates in macropores are certainly not identical—the two studied cases of surface and subsurface initiation approximate the envelope of the flow rate distribution in continuous earthworm macropores.

Acknowledgements

This work was funded by the Swiss Federal Institute of Technology in Zürich within the project ‘Investigation of the water exchange mechanisms between preferential flow paths and the soil matrix’. We thank Jeff McDonnell, Kerstin Stahl, and Brian McGlynn for improving the final manuscript.

References

Andreini, M.S., Steenhuis, T.S., 1990. Preferential paths of flow under conventional and conservation tillage. Geoderma 46, 85–102.

Aurenhammer, F., 1991. Voronoi diagrams-a survey of a fundamental geometric data structure. ACM Computing Surveys 23 (3), 345–405.

Beven, K., Germann, P., 1982. Macropores and water flow in soils. Water Resour. Res. 18 (5), 1311–1325.

Bouma, J., Belmans, C.F.M., Dekker, L.W., 1982. Water infiltration and redistribution in a silt loam subsoil with vertical worm channels. Soil Sci. Soc. Am. J. 46, 917–921.

Bowman, B.T., Brunke, R.R., Reynolds, W.D., Wall, G.J., 1994. Rainfall simulator-grid lysimeter system for solute transport studies using large, intact soil blocks. J. Environ. Qual. 23, 815–822.

Brimicombe, A.J., Tsui, P.H.Y., 2000. A variable resolution, geocomputational approach to the analysis of point patterns. Hydrological Processes 14, 2143–2155.

Buttle, J.M., House, D.A., 1997. Spatial variability of saturated hydraulic conductivity in shallow macroporous soils in a forested basin. J. Hydrol. 203, 127–142.

Deutsch, C.V., Journel, A.G., 1992. GSLIB-Geostatistical Software Library and Users Guide, Oxford University Press, New York.

Diggle, P.J., 1983. Statistical Analysis of Spatial Point Patterns, Academic Press, London.

Droogers, P., Stein, A., Bouma, J., de Boer, G., 1998. Parameters for describing soil macroporosity derived from staining patterns. Geoderma 83, 293–308.

Edwards, W.M., Shipitalo, M.J., Dick, W.A., Owens, L.B., 1992. Rainfall intensity affects transport of water and chemicals through macropores in no-till soil. Soil Sci. Soc. Am. J. 56, 52–58.

Ehlers, W., 1975. Observation on earthworm channels and infiltration on tilled and untilled loess soil. Soil Sci. 119 (3), 242–249.

Ela, S.D., Gupta, S.C., Rawls, W.J., 1992. Macropore and surface seal interactions affecting water infiltration into soils. Soil Sci. Soc. Am. J. 56, 714–721.

Faeh, A.O., Scherrer, S., Naef, F., 1997. A combined field and numerical approach to investigate flow processes in natural macroporous soils under extreme precipitation. Hydrol. Earth Syst. Sci. 4, 787–800.

Flühler, H., Durner, W., Flury, M., 1996. Lateral solute mixing processes-A key for understanding field-scale transport of water and solutes. Geoderma 70, 165–183.

Food and Agricultural Organization, 1974. FAO-UNESCO Soil Map of the World, 1:5000000, vol. I., Legend, Unesco, Paris.

Holmgren, P., 1984. Multiple flow direction algorithms for runoff modelling in grid based elevation models: an empirical evaluation. Hydrol. Processes 8, 327–334.

Huang, C.-H., 1998. Quantification of soil microtopography and surface roughness. In: Baveye, P., Parlange, J.-Y., Stewart, B.A. (Eds.), Fractals in soil science, CRC Press, Boca Raton.

Kiang, T., 1966. Random fragmentation in two and three dimensions. Zeitschrift für Astrophysik 64, 433–439.

Langmaack, M., Schrader, S., Rapp-Bernhardt, U., Kotzke, K., 1999. Quantitative analysis of earthworm burrow systems with respect to biological soil-structure regeneration after soil compaction. Biol. Fertil. Soils 28, 219–229.

Larson, M., 1999. Quantifying macropore flow effects on nitrate and pesticide leaching in a structured clay soil, Field Experiments and Modelling with the MACRO and SOILN Models, Swedish University of Agricultural Science.

Léonard, J., Esteves, M., Perrier, E., de Marsily, G., 1999. A spatialized overland flow approach for the modelling of large macropores influence on water infiltration. International Workshop of EurAgEng's Field of Interest on Soil and Water, Leuven, 313–322.

Léonard, J., Perrier, E., de Marsily, G., 2001. A model for simulating the influence of a spatial distribution of large circular macropores on surface runoff. Water Resour. Res. 37 (12), 3217–3225.

Li, Y., Ghodrati, M., 1997. Preferential transport of solute through soil columns containing constructed macropores. Soil Sci. Soc. Am. J. 61, 1308–1317.

Munyankusi, E., Gupta, S.C., Moncrief, J.F., Berry, E.C., 1994. Earthworm macropores and preferential transport in a long-term manure applied typic Hapludalf. J. Environ. Qual. 23, 773–784.

Phillips, R.E., Quisenberry, V.L., Zeleznik, J.M., Dunn, G.H., 1989. Mechanism of water entry into simulated macropores. Soil Sci. Soc. Am. J. 53 (6), 1629–1635.

Quinn, P.F., Beven, K.J., Chevallier, P., Planchon, O., 1991. The prediction of hillslope flow paths for distributed hydrological modelling using digital terrain models. Hydrol. Processes 5, 59–79.

Quisenberry, V.L., Phillips, R.E., Zelenzik, J.M., 1994. Spatial distribution of water and chloride macropore flow in a well-structured soil. Soil Sci. Soc. Am. J. 58, 1294–1300.

Schaap, M.G., Leij, F.J., 2000. Inproved prediction of unsaturated hydraulic conductivity with the Mualem-van Genuchten model. Soil Sci. Soc. Am. J. 64, 843–851.

Shipitalo, M.J., Edwards, W.M., 1996. Effects of initial water content on macropore-matrix flow and transport of surface-applied chemicals. J. Environ. Qual. 25 (4), 662–670.

Shipitalo, M.J., Edwards, W.M., Dick, W.A., Owens, L.B., 1990. Initial storm effects on macropore transport of surface-applied chemicals in no-till soil. Soil Sci. Soc. Am. J. 54 (6), 1530–1536.

Shipitalo, M.J., Gibbs, F., 2000. Potential of earthworm burrows to transmit injected animal wastes to tile drain. Soil Sci. Soc. Am. J. 64, 2103–2109.

Smettem, K.R.J., Collis-George, N., 1985. Statistical characterization of soil biopores using a soil peel method. Geoderma 36, 27–36.

Soil Survey Staff, 1951. Soil survey manual, US Department of Agriculture Handbook, 18.

Stein, A. (Ed.), 1999. Spatial Statistics for Remote Sensing, Kluwer, Dordrecht.

Syers, J.K., Springett, J.A., 1983. Earthworm ecology in grassland soils. In: Satchell, J.E., (Ed.), Earthworm Ecology, Chapman and Hall, London.

Trojan, M.D., Linden, D.R., 1992. Microrelief and rainfall effects on water and solute movement in earthworm burrows. Soil Sci. Soc. Am. J. 56, 727–733.

Trojan, M.D., Linden, D.R., 1998. Macroporosity and hydraulic properties of earthworm-affected soils as influenced by tillage and residue management. Soil Sci. Soc. Am. J. 62 (6), 1687–1692.

Wang, D., Norman, J.M., Lowery, B., McSweeney, K., 1994. Nondestructive determination of hydrogeometrical characteristics of soil macropores. Soil Sci. Soc. Am. J. 58 (2), 294–303.

Weiler, M., 2001. Mechanisms controlling macropore flow during infiltration-dye tracer experiments and simulations. Diss. ETHZ No. 14237, Zürich, Switzerland. http://e-collection.ethbib.ethz.ch/cgi-bin/show.pl?type = diss&nr = 14237.

Weiler, M., 2003. A new approach to describe infiltration into soils containing macropores. Water Resour. Res. in review.

Weiler, M., Naef, F., 2003. An experimental tracer study of the role of macropores in infiltration in grassland soils. Hydrol. Processes in press.

Weiler, M., Naef, F., Leibundgut, C., 1998. Study of runoff generation on hillslopes using tracer experiments and physically based numerical model. IAHS Publications 248, 353–360.

Wigmosta, M.S., Lettenmaier, D.P., 1999. A comparison of simplified methods for routing topographically driven subsurface flow. Water Resour. Res. 35, 255–264.

Zehe, E., Flühler, H., 2001. Slope scale variation of flow patterns in soil profiles. J. Hydrol. 247, 116–132.